

See discussions, stats, and author profiles for this publication at: <https://www.researchgate.net/publication/332326149>

Implementation and configuration of GB-SAR for landslide monitoring: Case study in Minami-Aso, Kumamoto

Article in Exploration Geophysics · March 2019

DOI: 10.1080/08123985.2019.1588069

CITATIONS

0

READS

50

5 authors, including:



Amila Karunathilake

Tohoku University

8 PUBLICATIONS 2 CITATIONS

[SEE PROFILE](#)



Lilong Zou

University of West London

20 PUBLICATIONS 32 CITATIONS

[SEE PROFILE](#)

Some of the authors of this publication are also working on these related projects:



The deformation monitoring of airport runway and taxing way by fully polarimetric GBSAR system [View project](#)



The research project on “Monitoring by using Ground-Base Synthetic Aperture Radar and Array-type Ground Penetrating Radar” under the support of Cross-ministerial Strategic Promotion Program (SIP) by the Japanese Government. [View project](#)



Implementation and configuration of GB-SAR for landslide monitoring: case study in Minami-Aso, Kumamoto

Amila Karunathilake, Lilog Zou, Kazutaka Kikuta, Masahiko Nishimoto & Motoyuki Sato

To cite this article: Amila Karunathilake, Lilog Zou, Kazutaka Kikuta, Masahiko Nishimoto & Motoyuki Sato (2019) Implementation and configuration of GB-SAR for landslide monitoring: case study in Minami-Aso, Kumamoto, *Exploration Geophysics*, 50:2, 210-220, DOI: [10.1080/08123985.2019.1588069](https://doi.org/10.1080/08123985.2019.1588069)

To link to this article: <https://doi.org/10.1080/08123985.2019.1588069>



Published online: 09 Apr 2019.



Submit your article to this journal



Article views: 39



View Crossmark data



Implementation and configuration of GB-SAR for landslide monitoring: case study in Minami-Aso, Kumamoto

Amila Karunathilake ^a, Lilog Zou  ^b, Kazutaka Kikuta  ^b, Masahiko Nishimoto  ^c and Motoyuki Sato  ^b

^aGraduate School of Environmental Studies, Tohoku University, Sendai, Japan; ^bCentre for Northeast Asian Studies, Tohoku University, Sendai, Japan; ^cGraduate School of Science and Technology (Engineering), Kumamoto University, Kumamoto, Japan

ABSTRACT

In this paper, the applicability of ground-based synthetic aperture radar (GB-SAR) as an early warning system for landslide monitoring is discussed. The effectiveness of the differential interferometric SAR (DInSAR) technique used in GB-SAR depends strongly on the geography of the monitored location. Therefore, an assessment of the system compatibility to select the most appropriate remote monitoring method is essential prior to any hardware implementation. In the preliminary part of this study, a 3D model was created using a LiDAR survey, and proposed locations for GB-SAR installation were examined. A 3D simulation was carried out to estimate the illumination from each of the proposed GB-SAR locations. The proposed model increased the efficiency of the GB-SAR positioning by minimising installation cost and time. Hardware configuration parameters, such as platform height, maximum range, and the direction and view angle of the radar line of sight were estimated by considering the optimum reflected power and ground illumination. Unlike on flat terrain, deployment of GB-SAR in a mountainous area is challenging because of surface anomalies and continuous changes in meteorological parameters, such as atmospheric temperature, pressure and relative humidity. In this study, the experimental site was located 3 km from the Aso volcano, and the weather conditions in the Aso caldera became a critical factor in accurately estimating the interferometric phase. The presence of atmospheric artefacts also compromises the applicability of the classical DInSAR technique. Here, we minimised the atmospheric phase screen by estimating the optimum data acquisition interval from GB-SAR monitoring under extreme weather conditions. The developed methodologies were then used to design a new landslide early warning system that measures real-time displacement over an area of 1 km² within 10 s of scanning. This fully automatic monitoring system updates every 15 min and presents displacement information in a 3D interface. The system we have developed has been deployed for continuous monitoring of the mountainous environment of a road reconstruction site in Minami-Aso, Kumamoto, Japan where a large-scale landslide was triggered following the Kumamoto earthquake in 2016.

ARTICLE HISTORY

Received 1 February 2019
Accepted 2 February 2019

KEYWORDS

3D modelling; displacement; GIS; remote sensing; sensors

Introduction

Radar remote sensing techniques give accurate information for environmental monitoring. Synthetic aperture radar (SAR) sensors allow all-day data collection under any weather conditions. Compared with spaceborne and airborne radar remote sensing techniques, ground-based SAR (GB-SAR) can achieve higher spatial and temporal resolution. These key factors can give more timely information of displacement measurements, for example in landslide and land subsidence monitoring. The enormous damage caused by landslides can be reduced by using monitoring systems in mitigation strategies (Takahashi et al., 2013). The GB-SAR system, which operates in the Ku frequency band, is very sensitive to small deformations, ranging from sub-millimetre to millimetre in size. This sensitivity is achieved by exploiting the interferometric capability of centimetre-wavelength microwaves (Placidi et al., 2015). The displacement between any two acquisitions

is derived from the interferometric phase, which is given by the difference between the phases of any two measurements.

Unlike conventional ground displacement monitoring techniques, such as a GPS station, inclinometer meter or extensor meter (Gunathilake et al., 2002), the GB-SAR can obtain two-dimensional (2D) deformation maps of an area that might be inaccessible to any person or equipment for on-site installation. One GB-SAR system can be used to monitor displacement over a large area within a short period, which improves the effectiveness and efficiency of the whole monitoring process. In addition, less equipment and fewer frequent data acquisitions are required by the GB-SAR system compared with conventional point-by-point measurement techniques.

However, due to topographical irregularities in the target area, the system may not measure the obligatory area as expected. Consequently, the quality of the

received data and the efficiency of the equipment may also be affected. In this study, a new methodology was introduced to guide GB-SAR installation, based on a 3D model-assisted survey. In our proposed method, newly designed software tools (Karunathilake and Sato, 2017) are used to find the best installation location for the GB-SAR, as well as the optimum hardware configuration, to receive the maximum reflection from the area of interest, prior to on-site deployment. This approach should improve the quality of the received data and the operating efficacy of the equipment.

Further experiments were carried out to improve the quality of the interferometric phase observations. Rapid changes in atmospheric conditions in mountainous areas affect the temporal decorrelation of the interferograms. The estimated interferometric phase is compromised by an ambiguous phase change, which is not related to any real displacement observed at the target surface. To overcome this, the atmospheric phase compensation method has been used based on statistical analysis. These proposed methods were validated by applying them to a real-time landslide and early warning station installed in the Minami-Aso road reconstruction site in Kumamoto, Japan.

This paper is structured as follows. First, a description of the test site and the requirement of the GB-SAR as an early warning system are presented. The equipment used and its installation process are then described. The three-dimensional (3D) spatial modelling technique developed to estimate target illumination is presented. Next, interferometric phase distortion due to atmospheric effects is discussed. Thereafter, a new method is proposed to estimate the optimum data acquisition interval for GB-SAR. On the basis of the estimated displacement, implementation of the real-time monitoring system as a landslide early warning system is further described. Finally, the results of the developed system are discussed, and conclusions are drawn.

Test site and data set

The study area was located near the Futagawa–Hinagu fault zone, which extends northeast and southwest

along Kyushu Island, Japan. In April 2016, a large number of foreshocks and aftershocks were recorded in this region, and an M6.5 earthquake was recorded at 21:26 Japanese Standard Time (JST) on 14 April, followed by an M7.3 earthquake recorded at 01:25 JST on 16 April; the location is shown in Figure 1(a) (Dang et al., 2016). The number of earthquake-triggered landslides was impressive, and the largest was reported near National Road 57 (Yagi et al., 2016), as shown in Figure 1(b). The main debris flow of the landslide cut-off the main railway and main road from Kumamoto.

Emergency recovery projects were launched to remove the debris flow after the landslide as part of the disaster recovery plan. The soil layer deposited by the main debris flow near the foot of the mountain was removed by manned vehicles, whereas the unstable soil layer closer to the mountain peak was removed by unmanned vehicles controlled from a nearby remote station. The soil removal process was completed, and a road construction project was launched in January 2017. Because of the instability of the topsoil layer on the hillside, and the large number of recorded earthquakes in the fault zone, information about the stability of the surface soil layer was of significance for the safety of the workers involved in the road construction. Considering these, the GB-SAR remote sensing technique was identified as the best solution for the continuous observation of the stability of the risk zone.

GB-SAR installation

System setup

GB-SAR hardware

The GB-SAR system consists of a radar sensor, linear rail, power unit and operating personal computer (PC). The linear rail is mounted parallel to the ground surface to facilitate continuous movement of the radar unit by the mechanical system, as shown in Figure 2(a). The system works from an external AC power source, which continuously charges two batteries to keep the system steady and working through any sudden power failures in this remote region. The operating PC of the radar and the rail unit were connected to a high-speed internet

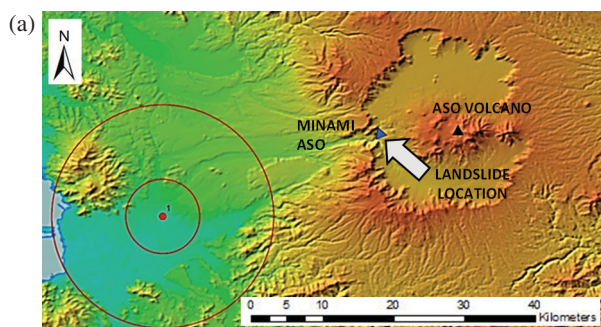


Figure 1. (a) Epicentre of the Kumamoto earthquake, 10 and 15 km buffer zones are depicted by red circles. (b) Photograph of the Minami-Aso landslide.

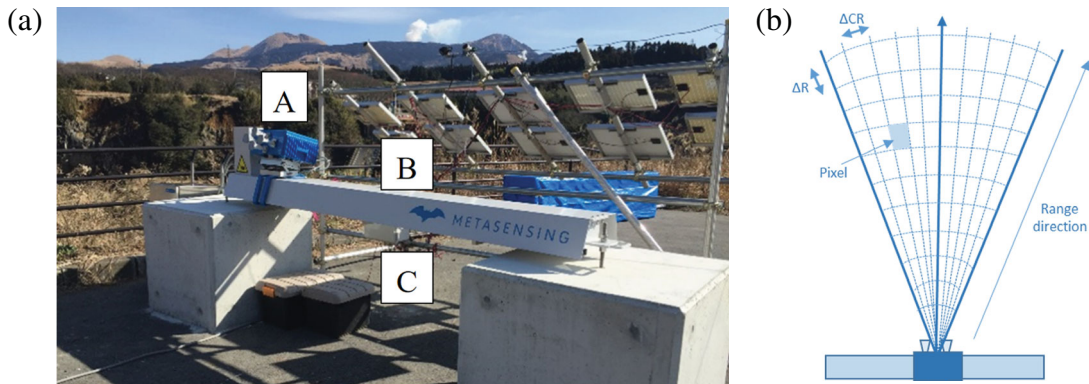


Figure 2. (a) GB-SAR system installed at Minami-Aso. The system includes the radar sensor (A), the linear rail (B) and the power supply unit (C). (b) SAR imaging geometry.

Table 1. Measurement parameters for GB-SAR system for the landslide monitoring.

System parameters	Magnitude
Centre frequency	17.2 GHz
Maximum range	4 km
Bandwidth	300 MHz
Rail length	1.8 m
Azimuth resolution	4.8 m/rad
Range resolution	0.5 m

connexion to transfer the acquired data to the processing PC, which was operated from Tohoku University, Miyagi Prefecture.

System parameters

The GB-SAR uses frequency modulated continuous wave technology. Figure 2(b) shows how a ground surface patch (Pixel) is defined in the range direction, ΔR , and in the cross-range direction, ΔCR . The system parameters are summarised in Table 1.

After data acquisition, a 2D SAR image is obtained by applying SAR processing (Fortuny-Guasch, 2009) to the acquired data. After transferring the data to the remote PC, the phase difference between two complex-valued SAR images was calculated. In GB-SAR, the differential phase can be projected directly into an equivalent range displacement or in other words, the deformation, Δd ,

$$\Delta\varphi_{(x,r)} = -\frac{4\pi}{\lambda} \Delta d_{(x,y)} \quad (1)$$

where λ is the reference wavelength of the transmitted signal and π is a constant. In deriving this equation, we assumed that the propagation properties of the transmission medium are homogeneous in the temporal domain. When the transmission medium remains constant for consecutive acquisitions, it can be interpreted as a line-of-sight physical displacement of the target. In a real application, this assumption is no longer valid, and atmospheric phase compensation must be applied to estimate the real displacement. After the atmospheric correction has been performed, the real-time displacement and displacement rate can be estimated from

the data. The real-time displacement of estimated stable points, coherent scatterers (CS), was projected onto a digital elevation model (DEM) to retrieve the real-time displacement from the 2D map. Furthermore, the displacement of critical locations, such as metal corner reflectors, was plotted automatically for continuous observation. The mean displacement was then calculated, and the displacement rate was estimated from the real-time data to send an early warning to the construction site.

Spatial model

Geographical information

Spatial distribution of the radiated signal is an indispensable factor for environmental monitoring systems. It provides significant information about equipment usability, prior to field installation. Following the catastrophic landslide in Kumamoto, the geography of the surrounding Minami-Aso area was unpredictably changed, and many places became inaccessible. After the first field observation survey, six locations (Loc 1 to Loc 6) were identified as possible sites for GB-SAR installation. Meanwhile, infrastructure such as transportation and electricity were shut off so equipment maintenance facilities were different in each place. As a result, a preliminary estimate of the equipment applicability was mandatory to reduce system deployment time and cost. The road reconstruction project was being actively carried out at the foot of the mountain. Hence, a more complex method to estimate the GB-SAR illumination prior to site deployment was required to minimise the calibration time for fast deployment in a disaster situation.

DEM

The western tip of the Aso caldera has a higher elevation. The highest summit on the mountainside was around 816 m. The proposed installation sites were located at an average altitude of ~ 400 m a.s.l. The lowest elevation was recorded at around 266 m where

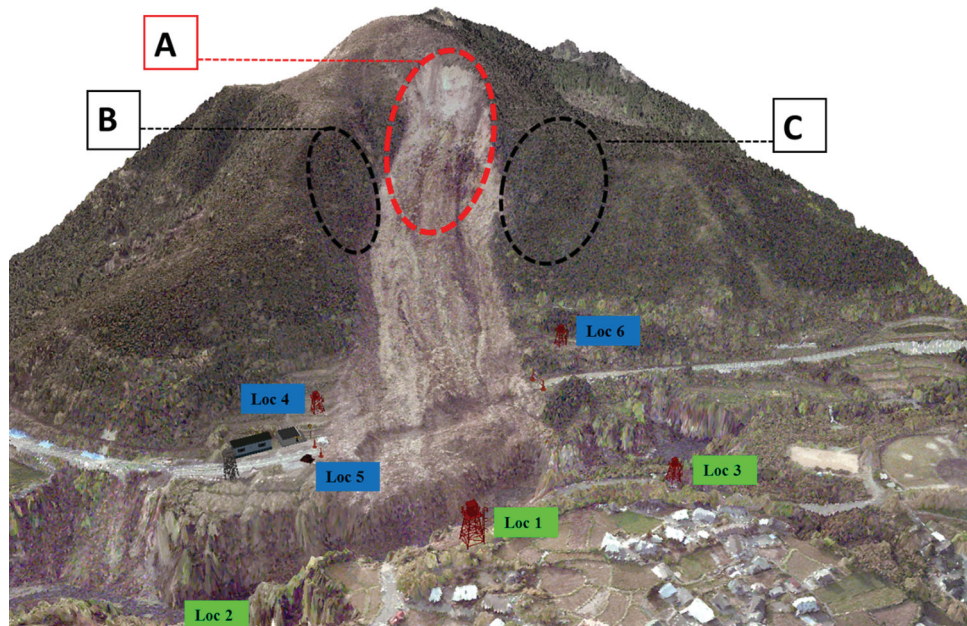


Figure 3. Spatial design of the 3D simulation model of the Minami-Aso landslide area.

the Kurokawa River flows. The riverbank near the landslide location has a steep slope with a sudden drop of ~ 80 m. Following the earthquake, the Ohashi Bridge that connects the two riverbanks collapsed, and access to the opposite side of the river was completely disconnected. A LiDAR survey was carried out in May 2016, after the earthquake. A DEM was generated with 30 cm pixel accuracy. This geocoded DEM model contained the pixel orientation in 3D. After the earthquake, the main debris flow flowed through dense forest. The surface soil layer on the mountain was divided into two layers according to the disaster recovery work.

3D model-assisted survey

The soil layer near the crown of the landslide and the surrounding area (area A in Figure 3) were prioritised. The remaining unstable soil layer in this area was removed initially by unmanned vehicles, which were operated from a remote station. This process was carried out systematically until December 2016. Starting from January 2017, the road reconstruction project was launched, and workers began from the foot of the mountain. Because of the instability of the top soil layer on the hillside and the number of recorded earthquakes in the fault zone, information on the stability of the surface soil layer and the newly created geological boundaries in areas B and C (Figure 3) were of significant importance for the safety of the workers involved in the daily road construction work. The proposed locations for GB-SAR installation are shown in the 3D model as Loc 1 to Loc 6, which are located on the left (blue) and right (green) sides of the Kurokawa River. These locations were selected by visual inspection during field observation. Because the area to be monitored is wide and site access was restricted due to the ongoing construction

work, selection of the location for the GB-SAR installation became a challenging task. Moreover, following the landslide, the geomorphology of the area had changed and most of the basic facilities, such as transportation and power supplies, were limited. Therefore, choosing locations for the system installation became even more important for optimum monitoring results, as well as for system maintenance work.

Estimation of GB-SAR illumination

Software tool design

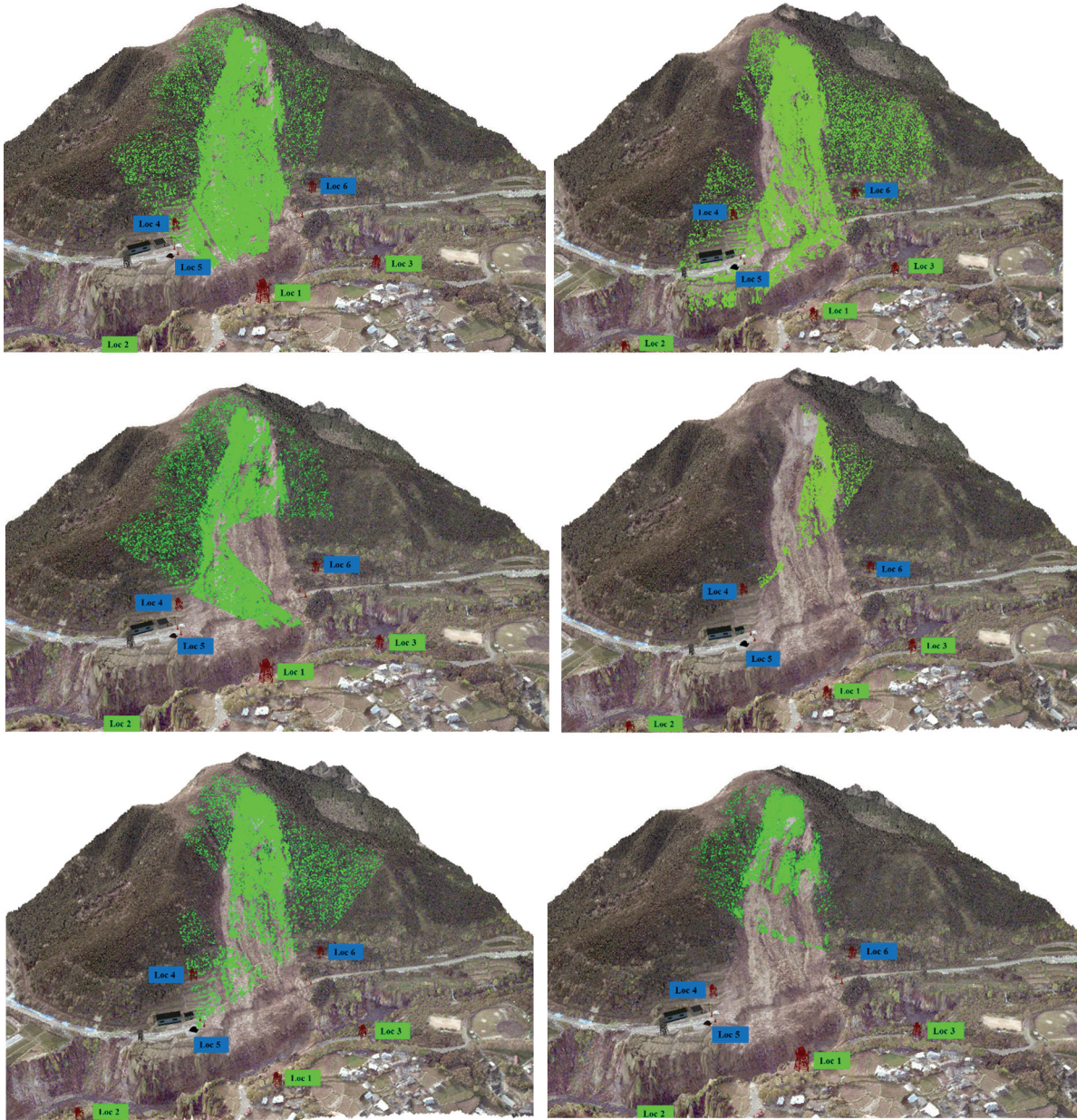
We developed a new software tool to extract spatial information from a terrestrial model on the Python platform, with Arcpy and Numpy libraries (Zandbergen, 2013). In this simulation, a DEM was created using the LiDAR survey, which was conducted 1 month after the landslide. This DEM information was used to calculate the orientation of each ground patch in the landslide area in three dimensions. The radiation pattern of the GB-SAR system was estimated in both the H-plane and the E-plane. A conical polygon area, which was based on the estimated radiation pattern, was further decomposed according to the range and azimuth resolution of the SAR image (Ulaby et al., 2014). A polygon grid at SAR pixel resolution was then used to extract spatial information from the DEM surface. Thereby, we were able to estimate the reflection angle for each of the ground patches for the proposed GB-SAR installation locations, and the corresponding ground illumination area was selected using radar coordinates (Karunathilake and Sato, 2017).

Estimation of optimum system parameters

The expected illumination from each location, Loc 1 to Loc 6, was estimated by using the software tools

Table 2. Estimated parameters for GB-SAR installation.

Location	Latitude	Longitude	Radar range (m)	Base height (m)	Azimuth angle (°)	View angle (°)	Illumination area (%)
Loc 1	32.883945°N	130.990160°E	1000	8	290	15	86.4
Loc 2	32.880030°N	130.989195°E	1000	10	300	15	65.0
Loc 3	32.886185°N	130.989912°E	1000	10	265	15	65.0
Loc 4	32.883408°N	130.986888°E	900	7	310	30	55.0
Loc 5	32.882468°N	130.987070°E	900	2	315	23	80.5
Loc 6	32.886487°N	130.987352°E	900	7	265	15	45.5

**Figure 4.** Estimated illumination, depicted in green, from each location (a) Loc 1 (b) Loc 2 (c) Loc 3 (d) Loc 4 (e) Loc 5 (f) Loc 6.

discussed above, and the simulation results are summarised in Table 2. The estimated illumination was geocoded by the local coordinate system and projected onto a 3D model. Figure 4 shows the expected illumination at each of the proposed installation locations. Loc 5 was selected for system installation after considering the estimated illumination at the target zones. The location also stood out due to the accessibility to the maintenance work and electricity supply, as well as other

infrastructure facilities, which were very important for the real-time monitoring.

The GB-SAR system was installed, and data acquisition started from mid-January 2017. The linear rail was mounted on 1.5 m rigid concrete blocks to achieve the necessary height for a stable platform. The system was oriented in the 315° direction, parallel to the installation terrain. The view (tilt) angle of the radar sensor was fixed to 23° in the vertical plane. The system was

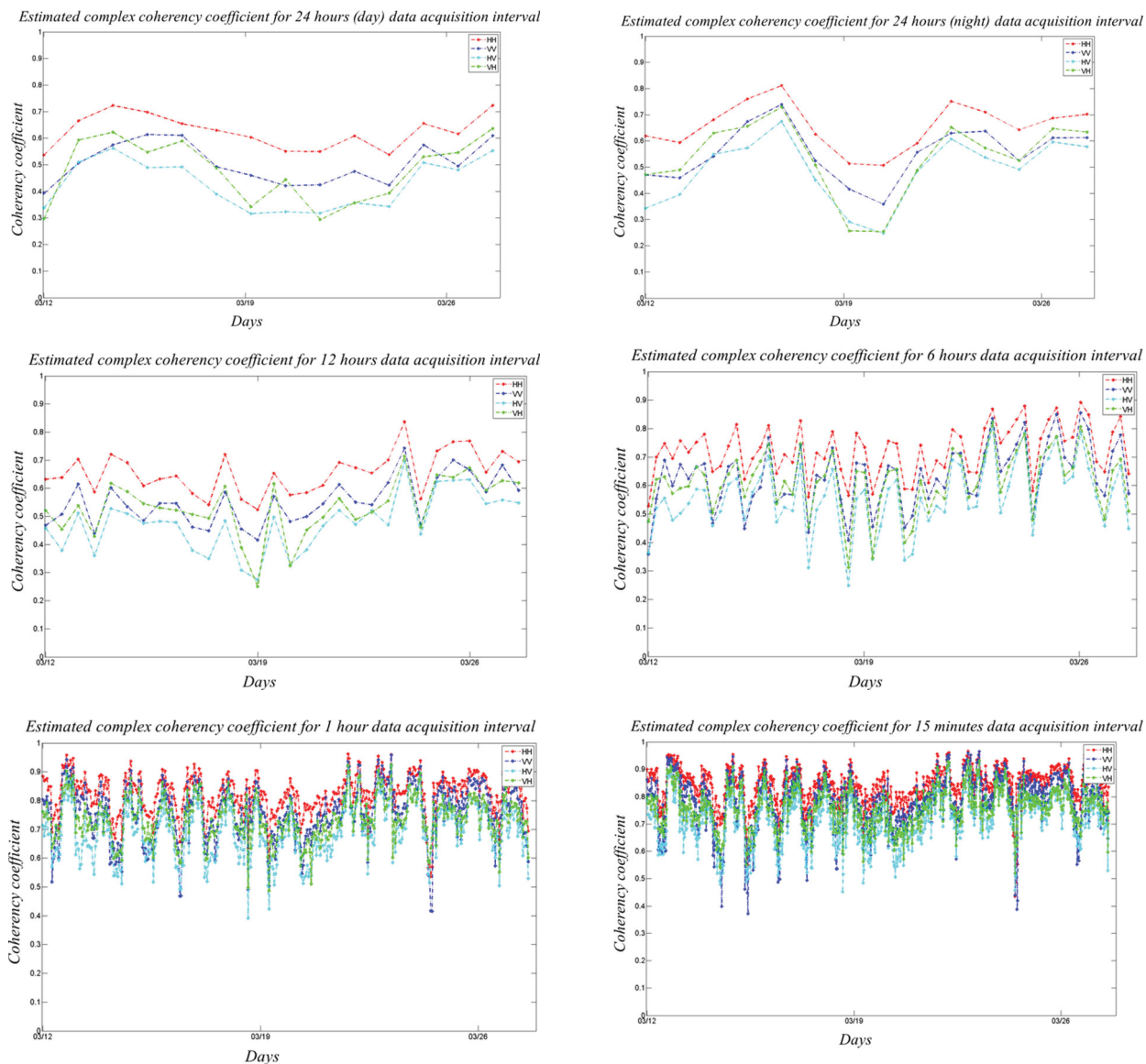


Figure 5. Complex coherence estimation for the GB-SAR data acquisition interval: (a) 1 day data (night-time); (b) 1 day (day time); (c) 12 h; (d) 6 h; (e) 30 min; and (f) 15 min.

calibrated, and sudden atmospheric changes showed a large influence on the interferometric phase, which was compensated to accurately estimate the ground displacement.

GB-SAR configuration

Interferometric phase

Differential SAR interferometry works under coherent conditions where the received waveforms correlate with the SAR pair used for comparison. One of the benefits of a GB-SAR sensor is the possibility of adding repeated zero-baseline scans for differential measurements. Therefore, terms that usually affect differential coherence, such as image co-registration, baseline construction uncertainties and removal of residual errors by digital elevation modelling become negligible (Luzi et al., 2004).

However, the GB-SAR works on the Ku band and is highly sensitive to small-scale changes, which tend to decorrelate within the time frame and therefore complicate quantitative long-term analysis. The problem of phase wrapping is one of the main issues observed in long-range SAR interferograms. Typically, phase unwrapping is performed on data that have been regularly sampled and stored in 2D matrices (Nico et al., 2000; Stramaglia et al., 1999). Unwrapping the phase without ambiguity requires the absolute phase gradient of the true phase between adjacent samples to be less than a π phase change along the unwrapping path. Here, a multi-interferogram framework was used to identify highly coherent targets along a straight line from the radar sensor (line of sight), to overcome most of the difficulties related to phase unwrapping, and to discern the different signal that competes with the interferometric phase.

Complex coherency

The complex coherency of the interferograms describes the correlation between consecutive data acquisitions and is a vital measurement of where the phase is exploitable. It should be emphasised that the coherence serves as a quality measurement of both acquisitions. The complex coherence, γ_c , between two images is defined as (Hanssen, 2001),

$$\gamma_c = \frac{E\{M \cdot S^*\}}{\sqrt{E\{M \cdot M^*\} \cdot E\{S \cdot S^*\}}} \quad (2)$$

where M is the master image, S is a slave image of the interferogram and $E\{.\}$ is the statistical expectation. The coherence is defined by $\hat{\gamma}$, and its estimator as (Seymour and Cumming, 1994),

$$\hat{\gamma} = \frac{\frac{1}{n} \sum_{i=1}^n M_i \cdot S_i^*}{\sqrt{\frac{1}{n} \sum_{i=0}^n M_i M_i^* \frac{1}{n} \sum_{i=0}^n S_i S_i^*}} \quad (3)$$

Coherence values lie in the range [0, 1] with higher values being more coherent. The coherence decorrelates with time due to changes in the observed scene. Fixed material and its shape in a particular scene have a large effect on the estimated coherence level. Vegetation has low coherence due to its entropic nature, whereas solid materials, such as rock and manmade structures, maintain a high coherence over a longer period. Therefore, the complex coherency of consecutive interferograms is considered as a quantitative measure of estimated interferograms.

Temporal phase compensation

In this study, the observation area ranged up to 800 m, including the tree canopy and the soil layer exposed after the landslide. The data acquisition interval of the remotely operated GB-SAR system was considered a key factor in the displacement estimation, but it also determines the data transfer rate to the monitoring station. In an advanced system, it can be used to preserve the coherency of the interferometric phase to minimise the temporal decorrelation. The problem of phase wrapping due to wave propagation in the range direction can be minimised technically by selecting the optimum data acquisition interval. It will improve the quality of the interferograms and make reliable information for displacement monitoring.

The environment near the GB-SAR monitoring station in Minami-Aso became a notable factor due to the water vapour content in the atmosphere of the low-elevation area. The wind speed and direction caused sudden changes in humidity. This can be identified as a factor that contributes noticeably to variations in reflectivity due to the highly dynamic weather conditions

Table 3. Summary of the number of datasets.

Duration	Number of data sets
1 day (night)	16
1 day (day)	16
12 h	32
6 h	63
3 h	127
1 h	312
30 min	616
15 min	1231
10 min	2251
5 min	4501
1 min	9000

(Smith Jr and Weintraub, 1953; Alduchov and Eskridge, 1996).

Owing to the capability of the latest GB-SAR system, the data acquisition interval can be as short as 10 s. During the preliminary site observations, fast data acquisition was not only a necessity for real-time monitoring, but also it was more than appropriate. Thus, the data acquisition interval was tested for 24 h (during both the day and night) at intervals of up to 1 min during the system calibration period and the recorded data set is summarised in Table 3.

Complex coherency was estimated as a qualitative and quantitative parameter for the interferometric phase. Figure 5 illustrates the estimated complex coherence coefficient for each data acquisition interval in the sample data sets acquired from 12 to 27 March. This statistical estimation shows that $\hat{\gamma}_{mean}$ fluctuates widely for a long data acquisition interval. Apart from the number of data sets, the estimated $\hat{\gamma}_{mean}$ during the day is lower than that estimated during the night. This implies that the observed interferometric phase during the day is more inconsistent than at night in the sample data set. Furthermore, the estimated interferometric phase distortion due to environmental changes becomes more significant in the day than at night. The estimated $\hat{\gamma}_{mean}$ variation of the coherency during the data acquisition intervals of 1 day, 12 h, 6 h and up to 1 m are displayed in Figure 6. A higher coherency value (close to 1) was noticed for small data acquisition intervals, whereas it became weaker (close to 0.6) for larger data acquisition intervals. This observation indicates that the temporal decorrelation was changed significantly between the 24 h and 30 min intervals. The temporal decorrelation of the interferometric phase shows a high fluctuation in this region, which adversely affects the reliability of the phase estimation. The estimated $\hat{\gamma}_{mean}$ from 15 to 1 min data acquisition intervals has high coherency and remained stable for 15, 10, 5 and 1 min data acquisition intervals. Therefore, the 15 min data acquisition interval was fixed as the optimum data acquisition interval.

In the spatial domain, the conventional atmospheric phase removal process consisted of a linear phase ramp over the range axis, which could be estimated through a simple linear regression model. In areas with steep topographic variation, fluctuations in the atmospheric

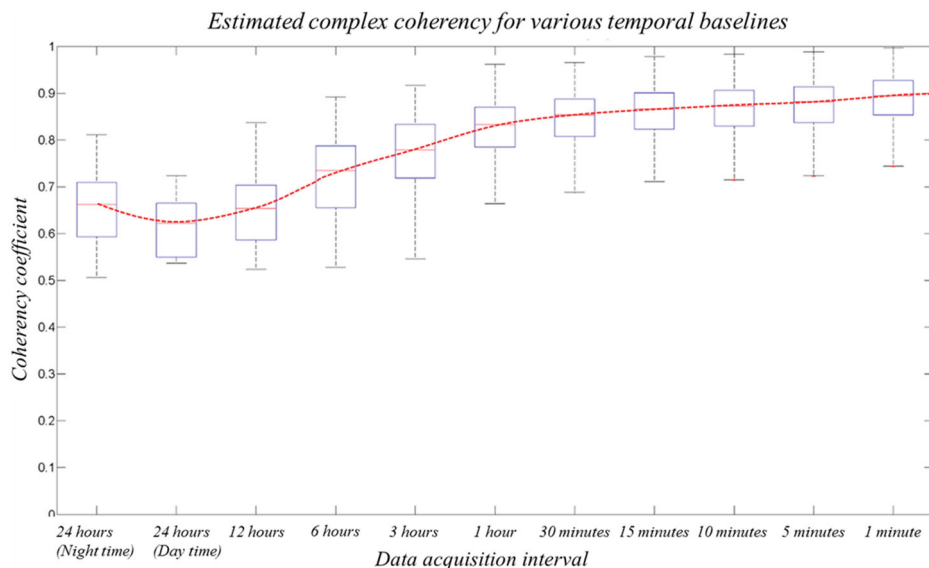


Figure 6. Interferometric phase quality estimation. The interferometric coherence change over the temporal baseline of 24 h at intervals of 1 min was summarised in the box plots.

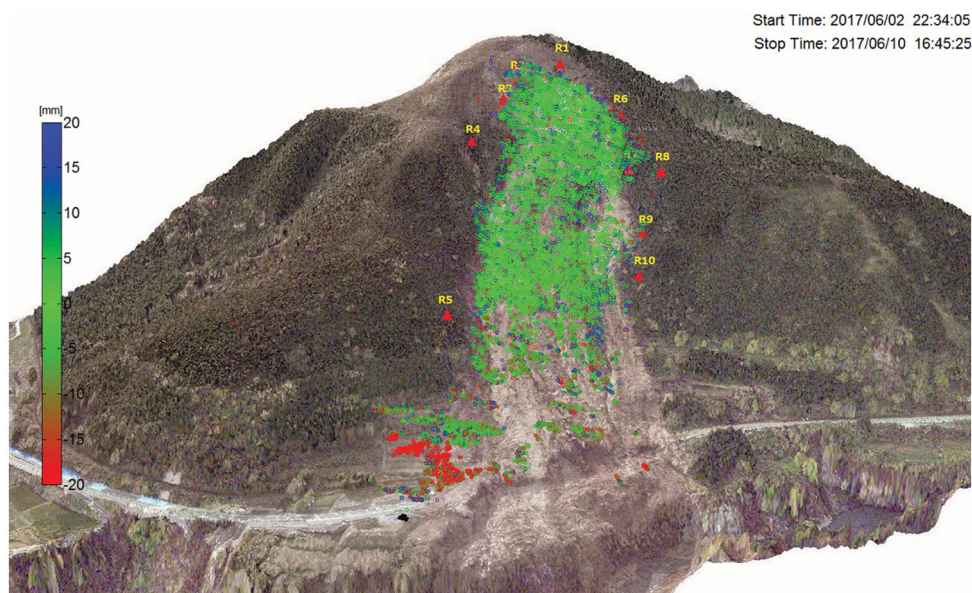


Figure 7. Observed real-time displacement over a 1-week period. The degree of displacement of the CS points is represented by the colour scale and the points are projected onto the DEM. The locations of the corner reflectors are marked in yellow as R1 to R10.

parameters, such as temperature, pressure and humidity, are observed in all directions. Hence, the assumption of spatial homogeneity in a single direction is no longer applicable. Therefore, a conventional linear regression model makes the phase a residual, which, in turn, makes an erroneous estimation of phase compensation. In this study, the atmospheric phase screen of each slope surface was separately evaluated and compensated.

Implementation of real-time monitoring system

Real-time 2D displacement

Pre-processing of the acquired data was done on site, and it was then transferred to Tohoku University via

the internet. After completing the advanced processing, the estimated displacement was retrieved on a 2D map, which was updated after every data acquisition. Figure 7 depicts the interface of the real-time monitoring PC. The reflected signal from the surface soil layer of the landslide is stable over time. Therefore, most of the CS points were distributed around this location. Each estimated CS point was projected onto the 3D DEM, and those locations were updated after every 15 min of data acquisition completed by the Minami-Aso GB-SAR. The radar measured the displacement in the line of sight direction, and the colour scale shows the displacement of each CS point. Blue represents movement towards the radar, whereas red shows movement in the opposite direction. Movement towards the radar can be identified as regions with a high potential for slope failure.

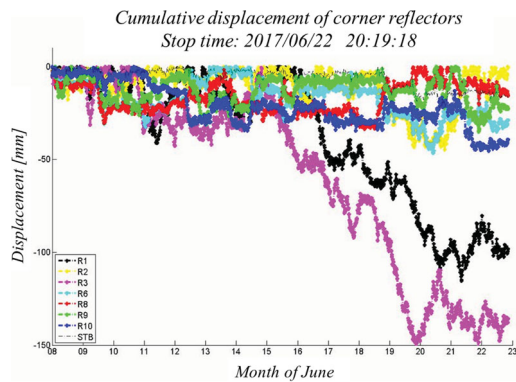


Figure 8. Observed displacement of the corner reflectors R1 to R10, and the movement of the ground point (STB) in the open soil layer of landslide.

In addition, due to the construction work carried out near the crown of the landslide, some loosely bound soil and rocks moved and accumulated in certain places on the slope. These regions of soil erosion can be identified by negative displacement along the radar line of sight. After construction of the road had started, most of the CS points near the radar were affected by the ongoing work and so were neglected. Displacement inside the forest canopy was strongly influenced by the stability of the untouched soil layer, which has lower coherency due to the frequent movement of tree leaves. Therefore, 10 corner reflectors were deployed and monitored remotely.

Real-time monitoring of corner reflectors

Real-time displacement of the corner reflectors was retrieved in the secondary interface, as shown in

Figure 8. It shows the real-time monitoring results from 7 of the 10 trihedral corner reflectors. Among those reflectors, R1 to R3 are located on the crown of the landslide. Following the catastrophic landslide, movement of the remaining ground area became a prime factor in the estimation of stability. Following the start of the rainy season in mid-June, reflectors R1 and R3, which were installed inside the forest, showed considerable movement.

Real-time alarm server

In practice, the necessity of an automatic early warning system was prioritised due to a sudden movement on the steep terrain, to send a prompt warning message to construction workers. As a result, the upper part of the radar illumination area was divided into 12 virtual clusters and the mean displacement of each cluster was calculated dynamically. From the data, if the mean cluster displacement exceeded a threshold level of 1 mm h^{-1} , the monitoring PC automatically detected the displacement rate and the corresponding cluster location, and generated an automatic email that was sent to the responsible parties to investigate the area by site inspection. The data-processing diagram of the system as implemented is shown in Figure 9. The system operated successfully, and a greater number of warnings were received during the rainy season.

Discussion

The estimated displacement along the radar line of sight can be used to identify location clusters that have

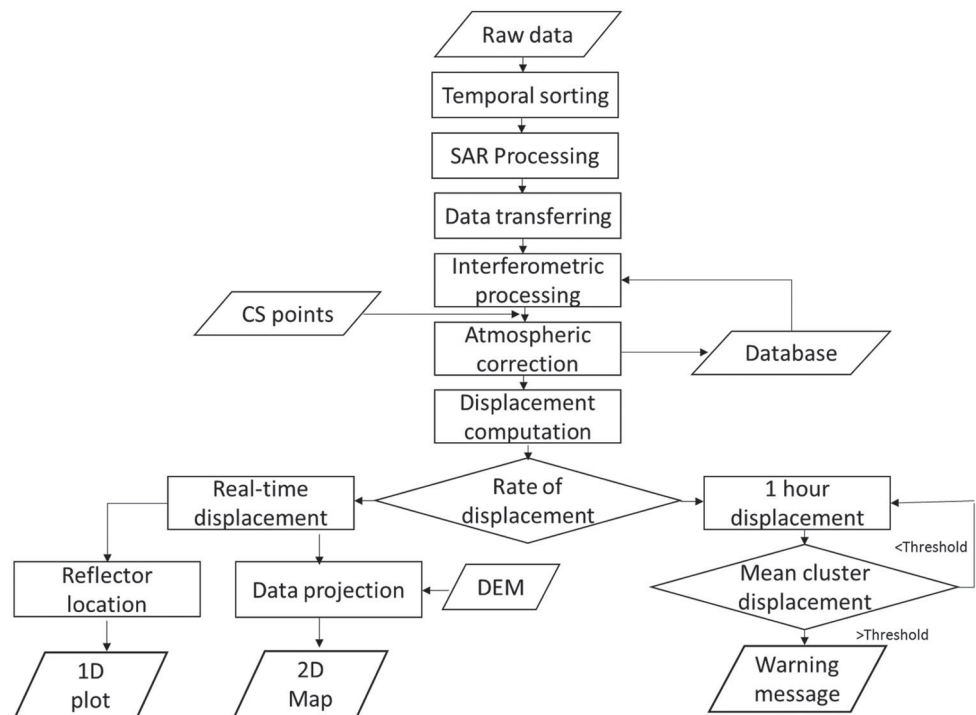


Figure 9. Data-processing diagram of the real-time landslide monitoring station.

high potential for triggering a landslide. This can be applied as a remote monitoring system for both urban and suburban environments. Because this can work as an independent stand-alone system, daily visits to the field, on-site readings and hardware maintenance are not necessary. Therefore, labour costs can be minimised and results monitoring automated. The spatial inhomogeneity of atmospheric influences was compensated, and accurate displacement measurements were estimated using phase information. Data transfer from the site to a remote processing station was done using an internet connexion via a WiFi router installed at the remote monitoring station. The transferred data were processed and retrieved as a 3D displacement map in real time. In the real-time monitoring system developed here, displacement data were presented so that they could be understood by both specialists and non-specialists. Hence, the complete monitoring process becomes affordable for a number of scientific and industrial applications. The system settings can be further improved according to the desired application. In this study, estimation of the direction of movement of a landslide was challenging, because it depends on the aspect angle of the existing slope surface, which needs further testing. Displacement inside the forest was evaluated in real-time by the coherent reflection of deployed corner reflectors. However, the displacement of some reflectors (R4, R5 and R7) inside the forest could not be described accurately because of the random influence of the tree canopy; therefore, dealing with canopy effects has to be improved.

Conclusion

GB-SAR implementation and configuration strategies within a complex geomorphological environment are discussed in detail. New estimation tools were designed in the spatial domain to understand the spatial distribution of the radiated signal. A 3D simulation model was developed based on a LiDAR survey. The proposed 3D model-assisted survey is a promising tool for minimising equipment installation time and cost. It became useful for immediate system deployment. These tools were tested and applied to the area of the Minami-Aso landslide, which is located in a mountainous environment. The best location for the GB-SAR installation was proposed as Loc 5, and the optimum GB-SAR configuration was evaluated. Continuous data acquisition started from mid-January 2017. The influence of the atmospheric phase screen on DInSAR became a critical factor in the detection of displacements in Minami-Aso. Because of the complicated geomorphology of the area, the temporal variations in atmospheric parameters led to errors in the estimation of displacement measurements in the time and space domains. The influence of the temporal change in the atmospheric conditions was evaluated successfully by the interferometric phase

quality from the complex coherence of consecutive interferograms. The consistency of the interferometric phase was analysed and a 15 min data acquisition interval was proposed as optimum for data acquisition.

Acknowledgments

This work was supported by JSPS Grant-in Aid for Scientific Research (A) 26249058 and Tohoku University-NICT joint matching project.

ORCID

Amila Karunathilake  <http://orcid.org/0000-0001-5141-4420>
Motoyuki Sato  <http://orcid.org/0000-0003-3888-2523>

References

- Alduchov, O. A., and R. E. Eskridge. 1996. Improved Magnus form approximation of saturation vapor pressure. *Journal of applied meteorology* 35: 601–609.
- Dang, K., K. Sasa, H. Fukuoka, N. Sakai, Y. Sato, K. Takara, L. H. Quang, D. H. Loi, P. V. Tien, and N. D. Ha. 2016. Mechanism of two rapid and long-runout landslides in the 16 April 2016 Kumamoto earthquake using a ring-shear apparatus and computer simulation (LS-RAPID). *Recent Landslides, Springer-Verlag Berlin Heidelberg* 13: 1525–1530.
- Fortuny-Guasch, J. 2009. A Fast and accurate pseudo polar format radar imaging algorithm. *IEEE Transactions on Geoscience and Remote Sensing* 47: 1187–1196.
- Gunathilake, J., Y. Iwao, and T. Yamasaki. 2002. Relationship of the faulting to the creep movement of Iwakura landslide in Saga, Japan: *Landslides- Journal of Japan Landslide Society* 39: 212–223.
- Hanssen, R. F. 2001. *Radar interferometry: Data interpretation and error analysis*. Dordrecht, The Netherlands: Kluwer.
- Karunathilake, A., and M. Sato. 2017. 3D Model assisted survey to design and estimate ground based SAR illumination, 42nd Remote sensing symposium, Chiba, 35–38.
- Luzi, G., M. Pieraccini, D. Mecatti, L. Noferini, G. Guidi, F. Moia, and C. Atzeni. 2004. Ground-based radar interferometry for landslides monitoring: Atmospheric and instrumental decorrelation source on experimental data. *IEEE Transactions on Geoscience and Remote Sensing* 42: 2454–2466.
- Nico, G., G. Palubinskas, and M. Datcu. 2000. Bayesian approaches to phase unwrapping: theoretical study. *IEEE Transactions on Signal Processing* 48: 2545–2556.
- Placidi, S., A. Meta, L. Testa, and S. Rodelsperger. 2015. Monitoring structures with FastGBSAR. *Proc. IEEE Radar conference*, 435–439.
- Seymour, M. S., and I. G. Cumming. 1994. Maximum likelihood estimation for SAR interferometry," in Proc. IGARSS-Surface Atmospheric Remote Sensing: Technologies. *Data Analysis Interpretation* 4: 2272–2275.
- Smith, E. K., and S. Weintraub Jr. 1953. *The constant in the equation for atmospheric reflective index at Radio frequency*. Proc. The Institute of Radio Engineers (IRE) conference, 1035–1037.
- Stramaglia, S., G. Nico, F. Lovergine, and L. Guerriero. 1999. *InSAR phase unwrapping algorithm based on mean-field theory*. Geoscience and Remote Sensing Symposium, IGARSS '99 Proceedings, IEEE.
- Takahashi, K., M. Matsumoto, and M. Sato. 2013. Continuous observation of natural-disaster-affected area using

- ground-based SAR interferometry. *IEEE journal of selected topics in applied earth observation and remote sensing* 6: 1286–1294.
- Ulaby, F. T., and D. G. Long. 2014. *Microwave radar and radiometric remote sensing*. x: The University of Michigan Press.
- Yagi, Y., R. Okuwaki, B. Enescu, A. Kasahara, A. Miyakawa, and M. Otsubo. 2016. Rupture process of the 2016 Kumamoto earthquake in relation to the thermal structure around Aso volcano. *Earth, Planets and Space* (Springer) 68: 1–6.
- Zandbergen, P. A. 2013. *PYTHON Scripting for ArcGIS*. Redland: ESRI Press.